

Higher-order soft corrections to squark hadro-production

U. Langenfeld and S. Moch

*Deutsches Elektronensynchrotron DESY
Platanenallee 6, D-15738 Zeuthen, Germany*

Abstract

We present new predictions for the total cross section of squark pair-production at Tevatron and LHC through next-to-next-to-leading order within the Minimal Supersymmetric Standard Model. The results are based on the numerically dominant soft corrections. They are exact in all logarithmically enhanced terms near threshold, include the Coulomb corrections at two loops and exact scale dependence. We translate the increased total cross section at next-to-next-to-leading order into improved exclusion limits for squark masses and we investigate the scale dependence as well as the sensitivity on the parton luminosity.

1 Introduction

Supersymmetry offers an attractive way for possible extensions of the Standard Model. Its most popular incarnation for phenomenological studies is the Minimal Supersymmetric Standard Model (MSSM) which features a rather rich spectrum of new (heavy) particles. Active searches are currently being performed at the Tevatron and soon at LHC. Squarks and gluinos as scalar and spin-1/2 supersymmetric partners of quarks and gluons could be pair-produced at a hadron collider at sizable rates (assuming R -parity). So far, Tevatron (CDF and D0 collaboration [1–3]) has been providing lower limits on their masses depending on certain assumptions about the parameter space of the MSSM. At LHC in contrast, one expects for an initial luminosity of about 10fb^{-1} and typical values of the MSSM parameters 10^6 (2500) squark pairs for a mass of 300 GeV (1 TeV) [4, 5]. Given these large rates and the dedicated searches performed, it is natural to investigate the accuracy of the available theoretical predictions including quantum corrections.

With squarks (and gluinos) carrying color charge, it is not surprising that Quantum Chromodynamics (QCD) provides the dominant corrections to the production cross section. This fact was realized some time ago and led to the computation of the complete next-to-leading order (NLO) QCD corrections [6]. The upshot is a large increase of the rate in comparison to leading order (LO) QCD predictions along with a reduced scale dependence indicating the improved theoretical uncertainty. The origin of these large higher order QCD corrections in hadro-production of (heavy) colored particles is well known, since it is related to universal QCD dynamics. As a typical pattern so-called Sudakov logarithms show up which originate from soft gluon emission in regions of phase space near partonic threshold. They depend on the squark velocity $\beta = (1 - 4m_{\tilde{q}}^2/s)^{1/2}$ and become large for center-of-mass energies \sqrt{s} near threshold for squark pair-production, $s \simeq 4m_{\tilde{q}}^2$. Sudakov logarithms can be organized to all orders of perturbation theory by means of a threshold resummed cross section to a given logarithmic accuracy.

In this letter, we study soft gluon effects for the total cross section of squark hadro-production. We employ Sudakov resummation to generate approximate next-to-next-to-leading order (NNLO) QCD predictions which are accurate in all $\log(\beta)$ -enhanced terms at two loops. Moreover, we include the complete two-loop Coulomb corrections as well as the exact dependence on the renormalization and factorization scale. To that end, we largely follow a similar study for top-quark hadro-production at the Tevatron and the LHC [7, 8]. The importance of Sudakov resummation for the latter reaction has often been emphasized in the literature (see e.g. Ref. [9]). Squarks are generally believed to be heavier than top quarks, but light enough to be pair-produced at these colliders as well, so that the need for threshold resummation (and the technique) carries over from top-quark pair-production. Recently, the soft gluon resummation for squark and gluino hadro-production has been performed to next-to-leading logarithmic (NLL) accuracy in Ref. [10], and results compatible with ours were found.

The letter is organized as follows. We recall the dominant parton channels contributing to the cross section of squark pair-production. Then we discuss the NLO QCD corrections. For the latter, we have determined fits to the exact NLO scaling functions for representative choices of squark and gluino masses (presented in the Appendix). Next, we describe the steps necessary to achieve soft gluon resummation to next-to-next-to-leading logarithmic (NNLL) accuracy. Thereby, we focus on the differences with respect to the well-known procedure for top-quarks. We employ the resummed cross section to derive new (approximate) NNLO expressions for the scaling functions and analyze the dependence of the hadronic cross section on the scale and on parton distribution functions (PDFs). For the finite order expansion to NNLO, we find good apparent convergence properties

and a markedly improved stability of the total cross section with respect to scale variations. We give two examples, how our results translate into new limits on the squark masses.

2 Setting the stage

We focus on the inclusive hadronic cross section of hadro-production of squark pairs, $\sigma_{pp \rightarrow \tilde{q}\tilde{q}^* X}$ which is a function of the hadronic center-of-mass energy \sqrt{s} , the squark mass $m_{\tilde{q}}$, and the gluino mass $m_{\tilde{g}}$. In the standard factorization approach of perturbative QCD, it reads

$$\sigma_{pp \rightarrow \tilde{q}\tilde{q}^* X}(s, m_{\tilde{q}}^2, m_{\tilde{g}}^2) = \sum_{i,j=q,\bar{q},g} \int_{4m_{\tilde{q}}^2}^s d\hat{s} L_{ij}(\hat{s}, s, \mu_f^2) \hat{\sigma}_{ij \rightarrow \tilde{q}\tilde{q}^*}(\hat{s}, m_{\tilde{q}}^2, m_{\tilde{g}}^2, \mu_f^2, \mu_r^2), \quad (1)$$

where the parton luminosities L_{ij} are given as convolutions of the PDFs $f_{i/p}$ defined through

$$L_{ij}(\hat{s}, s, \mu_f^2) = \frac{1}{s} \int_{\hat{s}}^s \frac{dz}{z} f_{i/p}\left(\mu_f^2, \frac{z}{s}\right) f_{j/p}\left(\mu_f^2, \frac{\hat{s}}{z}\right). \quad (2)$$

Factorization and renormalization scales μ_f and μ_r are identified ($\mu_f = \mu_r \equiv \mu$) and the sum in Eq. (1) runs over all massless parton flavors ($n_f = 5$ for LHC and Tevatron). The hard parton scattering cross section $\hat{\sigma}_{ij \rightarrow \tilde{q}\tilde{q}^*}$ appearing in Eq. (1) receives at Born level contributions from the channels

$$gg \rightarrow \tilde{q}_k \tilde{q}_l^*, \quad (3)$$

$$q_i \bar{q}_j \rightarrow \tilde{q}_k \tilde{q}_l^*, \quad (4)$$

where i, j, k and l denote flavor indices. For the calculation of the hadronic cross section (1) in this paper, we always sum over all final state squark flavors allowed by quantum number conservation in proton-(anti)-proton scattering except for top-squarks (stops). The contributing diagrams are displayed in Fig. 1.

While the gluon fusion process (3) always leads to like flavor squark pairs ($k = l$) and identical chiralities (see e.g. Ref. [6] for details on the quantum numbers), a $q\bar{q}$ initial state leads to a more interesting flavor structure of the final state squark pair. For the $q\bar{q}$ -scattering process (4) we have final states with the same flavor structure if the flavors of the initial state are different ($i \neq j \Rightarrow i = k \wedge j = l$) due to a gluino exchange in the t -channel. Likewise, if the initial flavors are equal ($i = j$), then the final flavors may be different from the initial flavors, but the flavors of the $\tilde{q}\tilde{q}^*$ -pair are equal due to a gluon exchange in the s -channel ($i = j \Rightarrow k = l$). Moreover, if we keep the squark chirality as a second quantum number, we encounter a richer structure and much of the discussion (including soft corrections) carries over. For the subsequent study of NLO and approximate NNLO perturbative QCD, we restrict ourselves to cross sections summed over all possible final squark flavors and chiralities (L, R). The complete list of Born cross sections for different flavors and chiralities is presented in the Appendix.

For the processes of our interest, the total partonic Born cross sections $\hat{\sigma}^B$ are given by (see e.g.

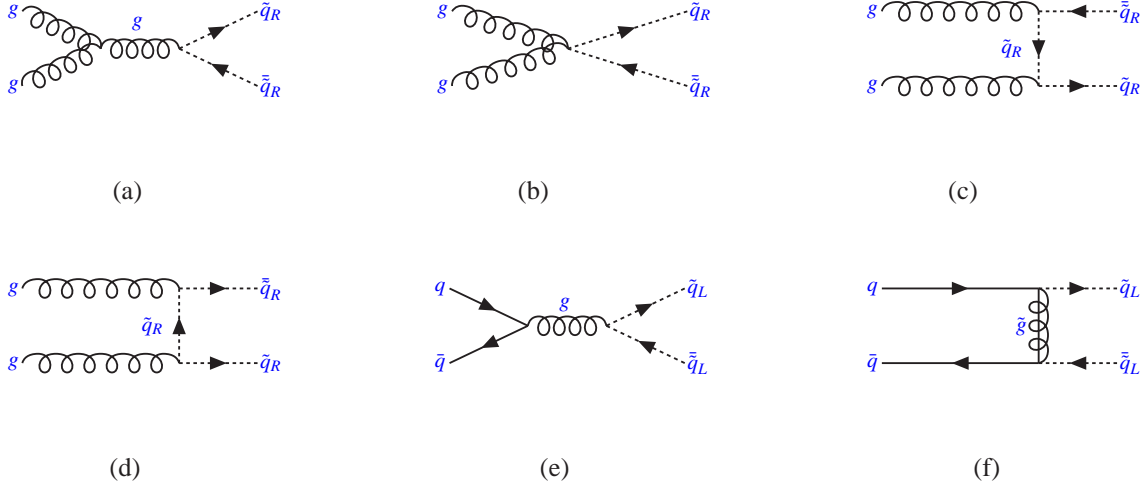


Figure 1: Contributing diagrams to the processes $gg \rightarrow \tilde{q}\bar{q}$ (diags. (a)–(d)) and $q_i\bar{q}_j \rightarrow \tilde{q}_i\bar{q}_j$ (diags. (e),(f)). Diagram (f) is proportional to the squark-gluino Yukawa coupling $\hat{\alpha}_s$ and introduces dependence on the gluino mass $m_{\tilde{g}}$.

Ref. [6]),

$$\hat{\sigma}_{gg \rightarrow \tilde{q}\bar{q}}^B(s, m_{\tilde{q}}^2) = \frac{\alpha_s^2}{m_{\tilde{q}}^2} \frac{n_f}{192} \pi (1 - \beta^2) \left[41\beta - 31\beta^3 + (17 - 18\beta^2 + \beta^4) \log \left(\frac{1 - \beta}{1 + \beta} \right) \right], \quad (5)$$

$$\begin{aligned} \hat{\sigma}_{q_i\bar{q}_j \rightarrow \tilde{q}\bar{q}}^B(s, m_{\tilde{q}}^2, m_{\tilde{g}}^2) &= \delta_{ij} n_f \frac{4\pi\alpha_s^2}{27s} \beta^3 \\ &\quad - \frac{4\pi\hat{\alpha}_s^2}{9s} \left[\beta \left(1 + \frac{(m_{\tilde{g}}^2 - m_{\tilde{q}}^2)^2}{m_{\tilde{g}}^2 s + (m_{\tilde{g}}^2 - m_{\tilde{q}}^2)^2} \right) + \left(1 + 2 \frac{m_{\tilde{g}}^2 - m_{\tilde{q}}^2}{s} \right) L_1 \right] \\ &\quad + \delta_{ij} \frac{4\pi\alpha_s \hat{\alpha}_s}{27s} \left[\beta \left(1 + 2 \frac{m_{\tilde{g}}^2 - m_{\tilde{q}}^2}{s} \right) + 2 \left(\frac{m_{\tilde{g}}^2}{s} + \frac{(m_{\tilde{g}}^2 - m_{\tilde{q}}^2)^2}{s^2} \right) L_1 \right], \end{aligned} \quad (6)$$

with the strong coupling constant α_s and the squark-gluino Yukawa coupling $\hat{\alpha}_s$ identical to α_s as required by supersymmetry (see the discussion below). Moreover, we have abbreviated

$$L_1 = \log \left(\frac{s + 2(m_{\tilde{g}}^2 - m_{\tilde{q}}^2) - s\beta}{s + 2(m_{\tilde{g}}^2 - m_{\tilde{q}}^2) + s\beta} \right), \quad (7)$$

where $\beta = (1 - 4m_{\tilde{q}}^2/s)^{1/2}$ is the squark velocity.

For the studies of higher order QCD corrections, the partonic cross section can be expressed in terms of scaling functions f_{ij} . For gluon fusion, we define

$$\hat{\sigma}_{gg \rightarrow \tilde{q}\bar{q}}(s, m_{\tilde{q}}^2) = \frac{\alpha_s^2}{m_{\tilde{q}}^2} \sum_{k=0}^{\infty} (4\pi\alpha_s)^k \sum_{l=0}^k f_{gg}^{(kl)}(\eta) \log^l \left(\frac{\mu^2}{m_{\tilde{q}}^2} \right), \quad (8)$$

and, likewise, for $q\bar{q}$ -scattering $f_{q_i\bar{q}_j}^{(kl)}$ with additional dependence on the gluino mass $m_{\tilde{g}}$, see Eq. (6). Here $\eta = s/(4m_{\tilde{q}}^2) - 1$ is a measure for the distance to the production threshold at $s = 4m_{\tilde{q}}^2$. The

NLO QCD corrections are known [6] although they are not available in analytical form (unlike the case of top-quark hadro-production [11]). Instead in Ref. [12], the authors present a numerical program called PROSPINO to calculate the complete hadronic cross section at NLO. We have used this program to extract values for the scaling functions $f_{gg}^{(10)}$, $f_{qq}^{(10)}$, and $f_{q_i q_j}^{(10)}$ (all terms proportional to $\log(\mu^2/m_q^2)$ will be discussed below). Subsequently, we have determined fits of these functions to per mille accuracy based on the following ansatz,

$$f_{gg}^{(10)} = \frac{7n_f}{192\pi}\beta \left(\frac{3}{2}\log^2(8\beta^2) - \frac{183}{28}\log(8\beta^2) + \frac{11\pi^2}{336\beta} \right) + h_{gg}(\beta), \quad (9)$$

$$f_{q_i \bar{q}_j}^{(10)} = \frac{4}{9\pi} \frac{m_g^2 m_q^2}{(m_g^2 + m_q^2)^2} \beta \left(\frac{2}{3}\log^2(8\beta^2) - \frac{11}{4}\log(8\beta^2) + \frac{7\pi^2}{48\beta} \right) + h_{q_i \bar{q}_j}(\beta). \quad (10)$$

The threshold logarithms $\log(\beta)$ as well as the Coulomb corrections ($\sim 1/\beta$) are kept exactly [6], while the fit function $h(\beta)$ is given in Eq. (A.11). These fits allow for an easy handling of the NLO QCD corrections in phenomenological applications.

The $\log(\beta)$ terms appearing in Eqs. (9) and (10) can be resummed systematically to all orders in perturbation theory employing the well established techniques (see e.g. Refs. [13–15]). The resummation typically proceeds in Mellin space after introducing moments N with respect to the variable $\rho = 4m_q^2/s$ as

$$\hat{\sigma}(N, m_q^2, m_g^2) = \int_0^1 d\rho \rho^{N-1} \hat{\sigma}(s, m_q^2, m_g^2). \quad (11)$$

For scattering reactions with non-trivial color exchange, one has to choose a suitable color basis for the total cross-section. It is convenient to select a decomposition according to color-singlet and color-octet final states,

$$\hat{\sigma}_{ij \rightarrow \bar{q}\bar{q}}(s, m_q^2, m_g^2) = \sum_{\mathbf{I}=1,8} \hat{\sigma}_{ij,\mathbf{I}}(s, m_q^2, m_g^2). \quad (12)$$

At Born level, we find the singlet component to be explicitly given by

$$\hat{\sigma}_{gg,1} = \frac{\alpha_s^2}{m_q^2} \frac{n_f \pi \rho}{4N_c(N_c^2 - 1)} \left[-\beta^3 + 2\beta + \frac{1}{2}(1 - \beta^4) \log\left(\frac{1 - \beta}{1 + \beta}\right) \right], \quad (13)$$

$$\hat{\sigma}_{q_i \bar{q}_j,1} = -\frac{\hat{\alpha}_s^2}{m_q^2} \frac{C_F^2 \pi}{2N_c^2} \rho \left[\beta \left(1 + \frac{(m_g^2 - m_q^2)^2}{m_g^2 s + (m_g^2 - m_q^2)^2} \right) + \left(1 + 2\frac{m_g^2 - m_q^2}{s} \right) L_1 \right], \quad (14)$$

and the octet terms $\hat{\sigma}_{ij,8}$ can be easily derived from Eqs. (3) and (4). The resummed cross sections (defined in the $\overline{\text{MS}}$ -scheme) for the individual color structures of the scattering process are then obtained as single exponentials in Mellin-space,

$$\frac{\hat{\sigma}_{ij,\mathbf{I}}(N, m_q^2, m_g^2)}{\hat{\sigma}_{ij,\mathbf{I}}^B(N, m_q^2, m_g^2)} = g_{ij,\mathbf{I}}^0(m_q^2, m_g^2) \cdot \exp(G_{ij,\mathbf{I}}(N+1)) + O(N^{-1} \log^n N), \quad (15)$$

where all dependence on the renormalization and factorization scale μ_r and μ_f is suppressed and the respective Born term is denoted $\hat{\sigma}_{ij,\mathbf{I}}^B$. The exponent $G_{ij,\mathbf{I}}$ contains all large Sudakov logarithms

$\log^k N$ and the resummed cross section (15) is accurate up to terms which vanish as a power for large Mellin- N . To NNLL accuracy, $G_{ij,\mathbf{I}}$ is commonly written as

$$G_{ij,\mathbf{I}}(N) = \log N \cdot g_{ij}^1(\lambda) + g_{ij,\mathbf{I}}^2(\lambda) + \frac{\alpha_s}{4\pi} g_{ij,\mathbf{I}}^3(\lambda) + \dots, \quad (16)$$

where $\lambda = \beta_0 \log N \alpha_s / (4\pi)$. The functions g_{ij}^k for the singlet and octet color structures are explicitly given in Ref. [7] and can be taken over from the case of top-quark hadro-production (see also Ref. [10] for the results to NLL accuracy). All g_{ij}^k , $k = 0, \dots, 3$ depend on a number of anomalous dimensions, i.e. the well-known cusp anomalous dimension A , the functions D and $D_{q\bar{q}}$ controlling soft emission, and the coefficients of the QCD β -function. At higher orders their precise expressions also depend on the chosen renormalization scheme, thus on the dynamical degrees of freedom. At the center-of-mass energies of Tevatron and LHC and for the mass ranges currently considered in MSSM phenomenology $m_{\tilde{q}}, m_{\tilde{g}} \simeq O(200 \text{ GeV} - 1 \text{ TeV})$, a scheme which decouples all heavy particles (top-quark, squarks, gluino) is appropriate. Thus, we are left with the Standard Model β -function coefficients $\beta_0 = 11 - 2/3 n_f$ and $\beta_1 = 102 - 38/3 n_f$ and the same expressions for the anomalous dimension A , D and $D_{q\bar{q}}$ as in the case of top-quark hadro-production (see Ref. [7]). Our scheme choice is in line with the exact NLO QCD calculation [6] to facilitate matching (see below). Throughout the paper, $m_{\tilde{q}}$ and $m_{\tilde{g}}$ denote pole masses.

Having Eq. (15) and all quantities necessary for its explicit evaluation at our disposal, we use the resummed cross section as a generating functional for the threshold approximation to the yet unknown NNLO QCD corrections, i.e. the inclusive partonic scaling functions $f_{ij}^{(20)}$ in Eq. (8). Substituting all numerical values and setting $n_f = 5$, we obtain for a representative choice of squark and gluino masses $m_{\tilde{q}} = 400 \text{ GeV}$ and $m_{\tilde{g}} = 500 \text{ GeV}$ in the $\overline{\text{MS}}$ -scheme the approximate NNLO results,

$$f_{gg}^{(20)} = \frac{f_{gg}^{(00)}}{(16\pi^2)^2} \left\{ 4608 \log^4 \beta - 1894.9144 \log^3 \beta + \left(-1309.5423 + 496.30011 \frac{1}{\beta} \right) \log^2 \beta \right. \\ \left. + \left(3523.9200 + 321.13660 \frac{1}{\beta} \right) \log \beta + 68.547138 \frac{1}{\beta^2} - 196.93242 \frac{1}{\beta} + C_{gg}^{(2)} \right\}, \quad (17)$$

$$f_{q\bar{q}}^{(20)} = \frac{f_{q\bar{q}}^{(00)}}{(16\pi^2)^2} \left\{ \frac{8192}{9} \log^4 \beta - 405.30701 \log^3 \beta + \left(567.40606 + 982.57395 \frac{1}{\beta} \right) \log^2 \beta \right. \\ \left. + \left(932.92034 + 336.72883 \frac{1}{\beta} \right) \log \beta + 205.64141 \frac{1}{\beta^2} - 634.79109 \frac{1}{\beta} + C_{q\bar{q}}^{(2)} \right\}, \quad (18)$$

$$f_{q_i \bar{q}_j}^{(20)} = \frac{f_{q_i \bar{q}_j}^{(00)}}{(16\pi^2)^2} \left\{ \frac{8192}{9} \log^4 \beta - 405.30701 \log^3 \beta + \left(450.41183 + 982.57395 \frac{1}{\beta} \right) \log^2 \beta \right. \\ \left. + \left(923.62614 + 336.72883 \frac{1}{\beta} \right) \log \beta + 205.64141 \frac{1}{\beta^2} - 634.79109 \frac{1}{\beta} + C_{q_i \bar{q}_j}^{(2)} \right\}, \quad (19)$$

where the coefficients of the $\log^4 \beta$ -terms are exact and we have used in the derivation the linearization of the Born functions,

$$f_{gg}^{(00)} = \frac{7n_f}{192} \pi \beta + O(\beta^3), \quad (20)$$

$$f_{q_i \bar{q}_j}^{(00)} = \frac{4}{9} \pi \beta \frac{m_{\tilde{g}}^2 m_{\tilde{q}}^2}{(m_{\tilde{g}}^2 + m_{\tilde{q}}^2)^2} + O(\beta^3). \quad (21)$$

For our phenomenological studies though, we have always substituted the full Born result for $f_{ij}^{(00)}$ in Eqs. (17)–(19).

A few comments on Eqs. (17)–(19) are in order here. The results are accurate to all powers in $\log(\beta)$ at two loops. This has been achieved by consistent matching of the resummed cross section to the exact NLO result for our choice of the masses $m_{\tilde{q}} = 400 \text{ GeV}$ and $m_{\tilde{g}} = 500 \text{ GeV}$. To that end, we have used our fits (9) and (10), specifically the constants a_1 of Eq. (A.11) as given in Tab. 3. These constants enter in the coefficients of $\log^2(\beta)$ and $\log(\beta)$ in Eqs. (17)–(19), i.e. the quadratic and linear logarithm. Strictly speaking, for the NLO matching separate constants are required for the singlet and octet color structures at NLO and for this reason the exact numerical coefficient of the term linear in $\log \beta$ will differ slightly. However, experience from studies for top-quark hadro-production shows this effect to be marginal [11] and well covered within our quoted overall uncertainty for the threshold approximation. On top of the threshold logarithms we have also added in Eqs. (17)–(19) the complete two-loop Coulomb corrections (as summarized e.g. in Ref. [7]). Finally, we comment on the presence of the squark-gluino Yukawa coupling $\hat{\alpha}_s$, which is identified with the strong coupling constant α_s as required by supersymmetry. In the $\overline{\text{MS}}$ -scheme this is achieved by a (finite) renormalization, which is correctly implemented at one-loop level by our matching procedure at NLO. At the two-loop level, the additional renormalization of $\hat{\alpha}_s$ would only affect the constant term $C_{q_i \bar{q}_j}^{(2)}$ in Eqs. (18), (19). Since we have no control over the latter, we set all two-loop constants $C_{ij}^{(2)}$ to zero in our phenomenological studies.

At this stage, it only remains to discuss those terms in Eq. (8) which describe scale dependence, i.e. the terms proportional to $\log(\mu^2/m_{\tilde{q}}^2)$. Through NNLO, this concerns $f_{ij}^{(11)}$, $f_{ij}^{(21)}$ and $f_{ij}^{(22)}$ which are entirely determined by renormalization group arguments (see. e.g. Refs. [16, 17]). They can be constructed with the help of lower order results, that is the scaling functions $f_{ij}^{(00)}$ and $f_{ij}^{(10)}$ and the splitting functions P_{ij} . The latter quantities govern the PDF evolution. They can be expanded as

$$P_{ij}(x) = \frac{\alpha_s}{4\pi} P_{ij}^{(0)}(x) + \left(\frac{\alpha_s}{4\pi} \right)^2 P_{ij}^{(1)}(x) + \dots, \quad (22)$$

and explicit expressions for the $P_{ij}^{(k)}$ can be found in Refs. [18, 19]. Following Refs. [16, 17] we can calculate the scale dependence of the partonic cross section. This yields the following result

$$f_{ij}^{(11)} = \frac{1}{16\pi^2} \left(2\beta_0 f_{ij}^{(00)} - f_{kj}^{(00)} \otimes P_{ki}^{(0)} - f_{ik}^{(00)} \otimes P_{kj}^{(0)} \right), \quad (23)$$

$$\begin{aligned} f_{ij}^{(21)} &= \frac{1}{(16\pi^2)^2} \left(2\beta_1 f_{ij}^{(00)} - f_{kj}^{(00)} \otimes P_{ki}^{(1)} - f_{ik}^{(00)} \otimes P_{kj}^{(1)} \right) \\ &\quad + \frac{1}{16\pi^2} \left(3\beta_0 f_{ij}^{(10)} - f_{kj}^{(10)} \otimes P_{ki}^{(0)} - f_{ik}^{(10)} \otimes P_{kj}^{(0)} \right), \end{aligned} \quad (24)$$

$$\begin{aligned} f_{ij}^{(22)} &= \frac{1}{(16\pi^2)^2} \left(f_{kl}^{(00)} \otimes P_{ki}^{(0)} \otimes P_{lj}^{(0)} + \frac{1}{2} f_{in}^{(00)} \otimes P_{nl}^{(0)} \otimes P_{lj}^{(0)} + \frac{1}{2} f_{nj}^{(00)} \otimes P_{nk}^{(0)} \otimes P_{ki}^{(0)} \right. \\ &\quad \left. + 3\beta_0^2 f_{ij}^{(00)} - \frac{5}{2} \beta_0 f_{ik}^{(00)} \otimes P_{kj}^{(0)} - \frac{5}{2} \beta_0 f_{kj}^{(00)} \otimes P_{ki}^{(0)} \right), \end{aligned} \quad (25)$$

where \otimes denotes the standard Mellin convolution, i.e. ordinary products in Mellin space under transformation (11). The summation over repeated indices for admissible parton contributions is implied, although for phenomenological applications we restrict ourselves in Eqs. (24) and (25) to the (numerically dominant) diagonal parton channels at two loops. Note, that the scale dependent two-loop contributions are exact at all energies also away from threshold. In this context, we remark that the usual definition of the splitting function P_{qg} (see e.g. Refs. [18, 19]) needs to be divided with a factor $2n_f$, because the standard definition implicitly contains a sum over all flavors. One other comment concerns the two-loop splitting function P_{qq} in Eq. (24). Obviously, only the flavor non-singlet splitting function $P_{qq} = P_{ns}^+$ enters the convolution (24) for the flavor non-singlet scaling function $f_{q_i\bar{q}_j}^{(21)}$ because flavor number is conserved. Likewise for the flavor singlet case $f_{q\bar{q}}^{(21)}$, the flavor singlet splitting function $P_{qq} = P_{ns}^+ + P_{ps}$ (i.e. the sum of non-singlet and pure-singlet) contributes. Finally, $f_{q_i\bar{q}_j}^{(00)}$ depends only on the ratio of the gluino and squark mass $r_q = m_{\tilde{g}}/m_{\tilde{q}}$. Therefore through Eqs. (23) and (25), the scaling functions $f_{q_i\bar{q}_j}^{(11)}$ and $f_{q_i\bar{q}_j}^{(22)}$ depend only on this ratio.

3 Numerical Results

Let us start to illustrate the phenomenological consequences. Throughout this paper, we assume for the gluino mass the relation $m_{\tilde{g}} = 1.25m_{\tilde{q}}$. Here our choice of parameters $m_{\tilde{q}} = 400\text{ GeV}$ and $m_{\tilde{g}} = 500\text{ GeV}$ as a reference point has been influenced by the current limits from direct searches. Thus far, lower limits on $m_{\tilde{q}}$ and $m_{\tilde{g}}$ are provided by Tevatron (CDF and D0 collaboration [1–3]) and an absolute lower limit of 379 GeV and 308 GeV, respectively, for the masses of squarks and the gluino in the mSUGRA framework ($A_0 = 0, \mu < 0, \tan\beta = 3$) has been quoted. Moreover, the non-stop-squarks are expected to be in a narrow mass range, because the Standard Model quarks are (nearly) massless and, in this case, nearly mass degenerated squarks are a property of mSUGRA. In the mSUGRA framework, the \tilde{t}_1 is lighter and the \tilde{t}_2 heavier than the other squarks and a typical particle spectrum can be found in Ref. [20] As announced already above, we have excluded stop quarks from our considerations here. Currently, the NLO QCD corrections to stop production are known [21] (see e.g. Ref. [22] for a search for the lightest stop \tilde{t}_1).

We display in Figs. 2 and 3 our results for the scaling functions as defined in Eq. (8) up to second order in α_s and separated according to the parton initial state gg and $q\bar{q}$. The results for $f_{ij}^{(20)}$, $f_{ij}^{(21)}$ and $f_{ij}^{(22)}$ are new. To illustrate the effect of threshold logarithms, we compare the scale independent functions $f_{ij}^{(00)}$, $f_{ij}^{(10)}$ and $f_{ij}^{(20)}$ directly in Figs. 2(e), 2(f) and 3(c). One clearly sees the effect of the large logarithms in β at low η giving rise to large perturbative corrections. At larger η , the results for $f_{ij}^{(20)}$ from Eqs. (17)–(19) vanish quickly and our approximation ceases to be valid for $\eta \gtrsim O(1 \dots 10)$.

Let us next investigate the consequences for the hadronic cross section (1) for squark pair-production at LHC and Tevatron. The necessary convolution of the parton scaling functions with the parton luminosity (2) emphasises the threshold region of phase space. The parton luminosity L_{ij} is steeply falling with increasing energies. Consequently, the total hadronic cross section is effectively saturated from partonic processes close to threshold with the kinematics being very similar to the case of top-quark hadro-production [7]. As an upshot, one can conclude, that our approximate NNLO result captures the numerically dominant part of the complete (yet unknown)

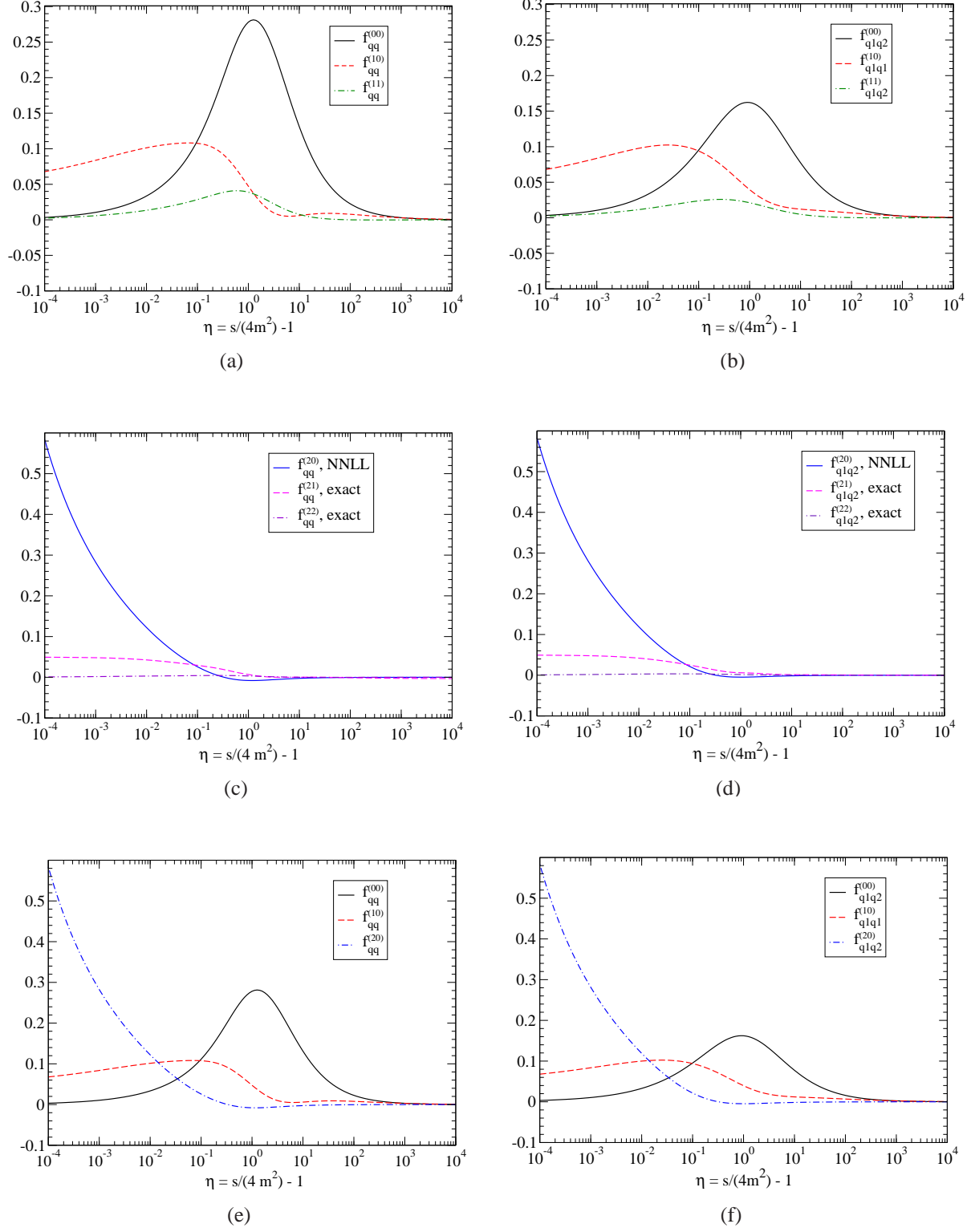
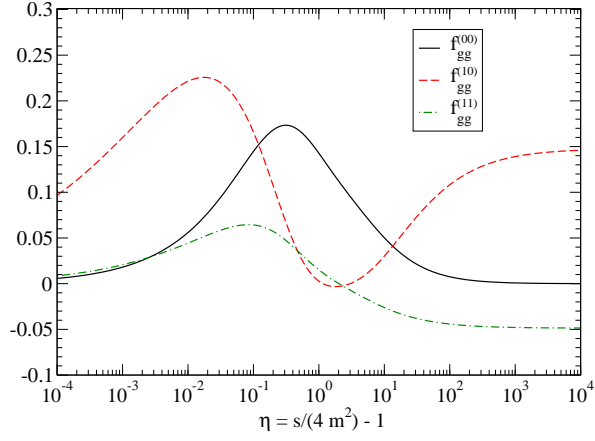
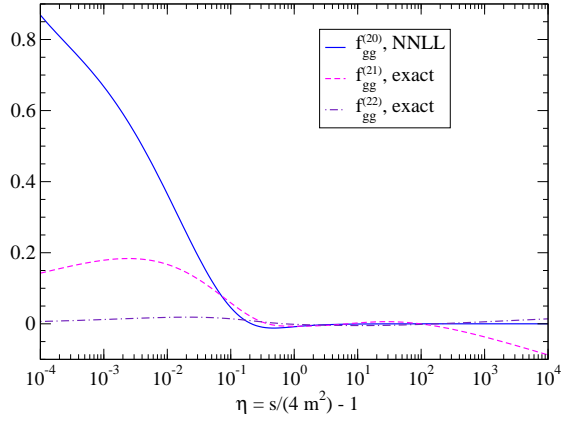


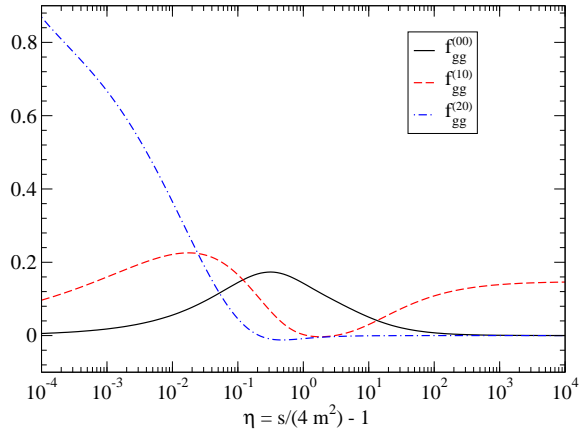
Figure 2: Scaling functions $f_{qq}^{(ij)}$ (left column) and $f_{q_l q_l}^{(ij)}$ (right column) with $i = 0 \dots 2$, $j \leq i$, for $m_{\tilde{q}} = 400 \text{ GeV}$ and $m_{\tilde{g}} = 500 \text{ GeV}$.



(a)



(b)



(c)

Figure 3: Scaling functions $f_{gg}^{(ij)}$ with $i = 0, 1, 2$ $j \leq i$.

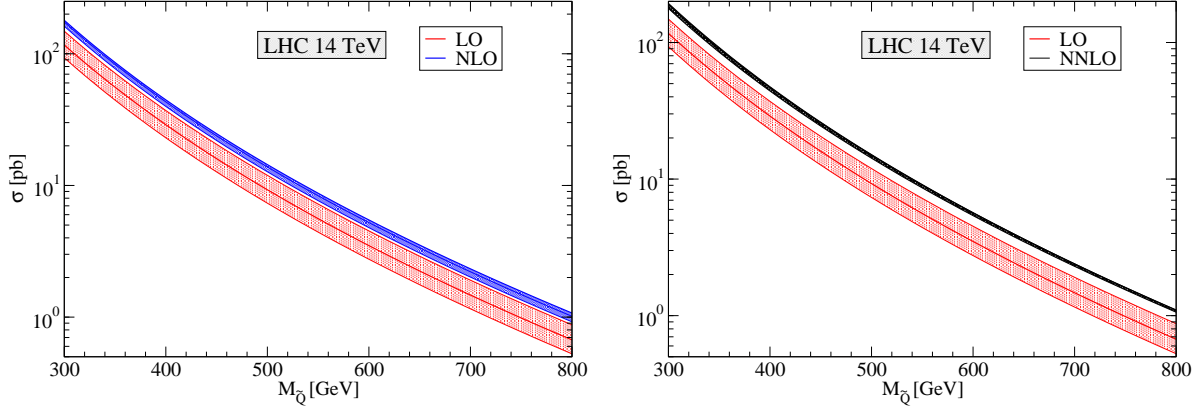


Figure 4: The total hadronic cross section for $pp \rightarrow \tilde{q}\tilde{q}^*$ at LHC with $\sqrt{s} = 14$ TeV to LO, NLO, and NNLO in QCD as function of the squark mass $m_{\tilde{q}}$. For the gluino mass we assume the relation $m_{\tilde{g}} = 1.25m_{\tilde{q}}$.

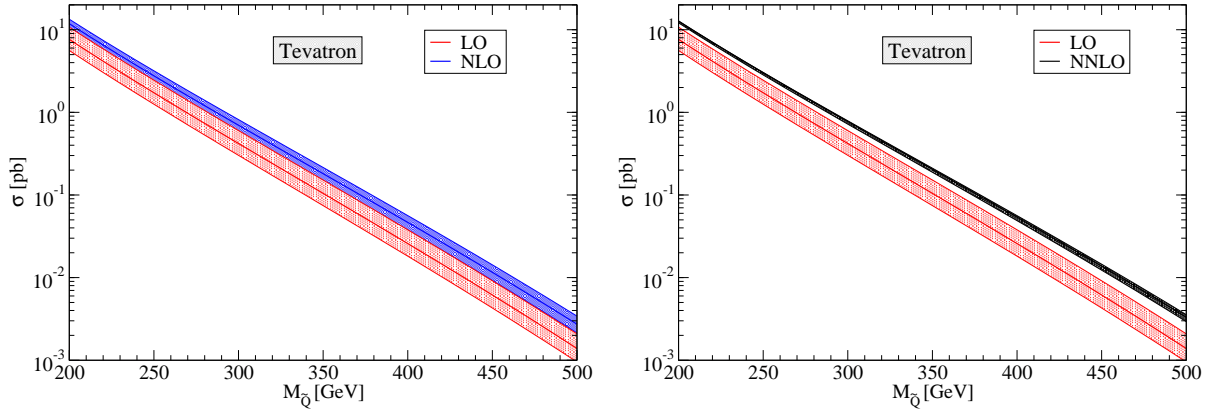


Figure 5: Same as Fig. 4 for Tevatron with $\sqrt{s} = 1.96$ TeV.

NNLO corrections. Eqs. (17)–(19) should thus represent a very reliable estimate.

In Fig. 4, we present the total cross section at the LHC as a function of the squark mass $m_{\tilde{q}}$. We use the PDF set CTEQ6.6 [23], if not stated otherwise. In the left figure, we show the LO and NLO QCD predictions for the cross sections along with their error bands due to the scale uncertainty for scale choices $x \equiv \mu/m_{\tilde{q}} = 2$ and $x = 1/2$. In Fig. 4 on the right, we show the same comparison for the LO and NNLO prediction. While the error band of the LO cross section is quite large (being entirely determined by the scale uncertainty of the strong coupling constant α_s) it shrinks when considering the NLO QCD prediction. For the cross section at NNLO accuracy, we apply our newly derived scaling functions $f_{ij}^{(20)}$, $f_{ij}^{(21)}$ and $f_{ij}^{(22)}$ of the previous Section. We observe how the error band contracts to a rather thin line, showing the significantly reduced scale uncertainty at this order of perturbation theory. In Tab. 1, we present numbers for the hadronic cross section for different squark masses and scales. The NLO cross section is increased by about 50% compared to the LO cross section, and likewise, the approximate NNLO cross section is increased by about 9% compared to the NLO cross section. As a direct phenomenological consequence we translate our result into shifts of the exclusion limits for the squark masses for one example. For instance, a cross section of 30 pb corresponds at LO, NLO, and NNLO to a squark mass of about 397 GeV,

430 GeV, and 437 GeV, respectively.

In Fig. 5, we present the same plot for the total cross section of $p\bar{p} \rightarrow \tilde{q}\tilde{q}^*$ at the Tevatron. Here, the cross section is more than two orders of magnitude smaller than at LHC due to the lower center-of-mass energy of Tevatron. Again, we observe improved stability of the perturbative predictions with respect to the scale variation. In Tab. 2, we give explicit values for the cross section. Again, the NNLO result implies new exclusion limits, for example for a cross section of 60 fb one comes up with a squark mass of about 370 GeV, 391 GeV and 396 GeV at LO, NLO, and NNLO, respectively.

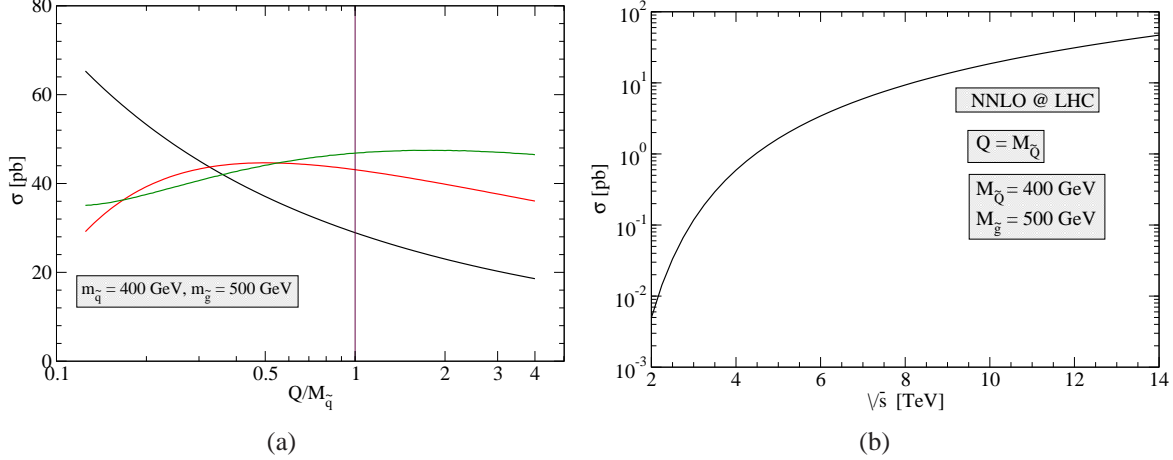


Figure 6: The total hadronic cross section for $pp \rightarrow \tilde{q}\tilde{q}^*$ at LHC as a function of the scale μ (left figure) and as a function of the center-of-mass energy \sqrt{s} (right figure) for the reference point. On the left hand side we compare the LO, NLO, and NNLO predictions for the μ dependence with $\sqrt{s} = 14$ TeV. On the right we display the \sqrt{s} dependence of our NNLO prediction at scale $\mu = m_{\tilde{q}}$.

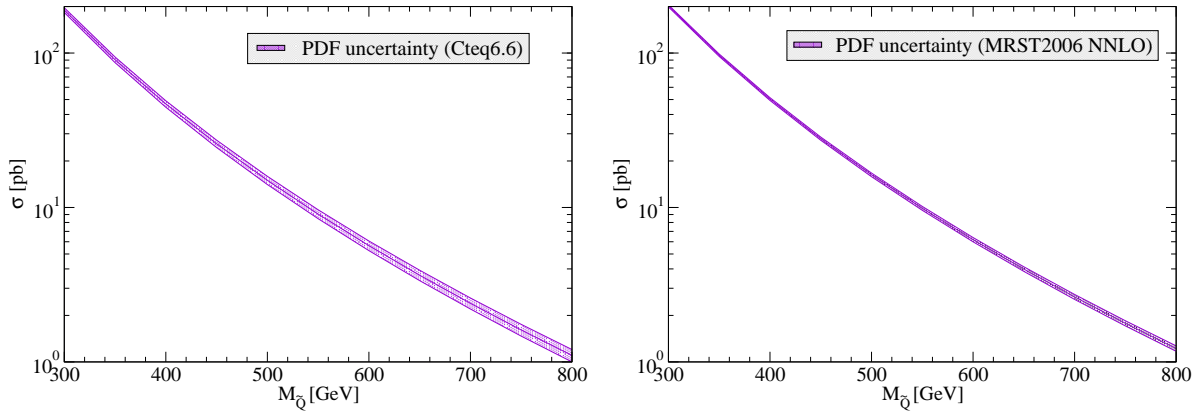


Figure 7: The PDF uncertainty of the NNLO cross section for the two PDF sets CTEQ6.6 [23] (left figure) and MRST2006nnlo [24] (right figure).

In order to illustrate the improved theoretical prediction due to the reduced scale dependence, we show in Fig. 6(a) the LO, NLO, and NNLO predictions for the cross section at LHC with $\sqrt{s} = 14$ TeV. One observes a decreasing dependence on μ with increasing order of perturbation

$m_{\tilde{q}}$ [GeV]	$\sigma(\text{LO})[\text{pb}]$			$\sigma(\text{NLO})[\text{pb}]$			$\sigma(\text{NNLO})[\text{pb}]$		
	$x = \frac{1}{2}$	$x = 1$	$x = 2$	$x = \frac{1}{2}$	$x = 1$	$x = 2$	$x = \frac{1}{2}$	$x = 1$	$x = 2$
300	148.4	116.6	93.2	179.5	174.2	161.9	177.4	189.8	193.4
400	37.1	28.9	23.0	44.6	43.1	39.8	44.1	46.8	47.4
500	11.9	9.3	7.3	14.4	13.8	12.7	14.2	15.0	15.1
600	4.51	3.49	2.75	5.47	5.22	4.78	5.39	5.66	5.68
700	1.91	1.47	1.16	2.33	2.21	2.01	2.29	2.40	2.40
800	0.87	0.67	0.53	1.07	1.01	0.92	1.06	1.10	1.10
900	0.43	0.33	0.25	0.53	0.50	0.45	0.52	0.54	0.53
1000	0.22	0.17	0.13	0.27	0.25	0.23	0.27	0.28	0.27

Table 1: Numerical values for the squark pair-production cross section at LHC with $\sqrt{s} = 14\text{TeV}$ and the CTEQ6.6 PDF set [23]. The QCD predictions are given at LO, NLO, and NNLO accuracy and for different squark masses and scales $x = \mu/m_{\tilde{q}}$.

theory. Within the commonly chosen scale interval $x = 0.5 \dots 2$, the LO, NLO, and NNLO cross section varies between 37pb and 23pb, 45pb and 40pb, and 44pb and 47pb, respectively (see Tab. 1). This amounts to a residual theoretical uncertainty of 3% for our approximate NNLO prediction.

The presently discussed schedule for the initial phase of LHC includes operation at a center-of-mass energy lower than 14TeV, a value of 10TeV has often quoted. For this reason, it is interesting to study the energy dependence of the cross section. In Fig. 6(b) we display our new approximate NNLO result as a function of the center-of-mass energy. We observe, for instance, at 10TeV a cross section of about 19pb for our reference point ($m_{\tilde{q}} = 400\text{GeV}$ and $m_{\tilde{g}} = 500\text{GeV}$) compared to 47pb for the design energy of 14TeV.

The final point of interest is the sensitivity to the parton luminosity and the associated uncertainty. In Fig. 7, we show the NNLO cross section for squark pair-production together with the error band due to the PDF uncertainties. We used two sets of PDFs: CTEQ6.6 (left figure, [23]) and MRST2006nnlo (right figure, [24]). At higher squark masses, the error on the cross section is significantly increased because the relevant phase space probes the gluon luminosity in the high- x region where the gluon PDF has a large uncertainty. Note that the quoted error for the MRST2006nnlo PDF set is significantly smaller than for the CTEQ6.6 set.

4 Conclusion and Summary

In this letter we have investigated the effect of higher order soft corrections on the total cross section for hadronic squark pair-production. These radiative corrections make up numerically for a large part of the higher order QCD effects. Starting from the existing NLO calculation we provide for the ease-of-use the NLO scaling functions $f_{ij}^{(10)}$ in the form of parametrizations which are accurate at the per mille level. Subsequently we have employed well established techniques for soft gluon resummation to derive new approximate NNLO results. Our two-loop expressions for the scaling functions $f_{ij}^{(20)}$ are exact in all logarithmically enhanced terms near threshold and they include the Coulomb corrections. All two-loop scaling functions $f_{ij}^{(21)}$ and $f_{ij}^{(22)}$ governing the scale dependence have been computed exactly using renormalization group arguments.

$m_{\tilde{q}}$ [GeV]	$\sigma(\text{LO})[\text{fb}]$			$\sigma(\text{NLO})[\text{fb}]$			$\sigma(\text{NNLO})[\text{fb}]$		
	$x = \frac{1}{2}$	$x = 1$	$x = 2$	$x = \frac{1}{2}$	$x = 1$	$x = 2$	$x = \frac{1}{2}$	$x = 1$	$x = 2$
200	10735.0	7641.1	5606.6	13394.7	11836.7	10091.7	12707.5	12749.7	12100.4
250	2450.5	1726.6	1254.3	3182.5	2766.6	2328.8	3043.4	3019.7	2835.0
300	602.4	419.9	301.9	816.9	698.6	580.4	789.9	775.2	720.1
350	151.8	104.6	74.4	215.2	181.1	148.4	211.0	204.9	188.2
400	37.9	25.8	18.2	56.3	46.6	37.7	56.2	53.9	48.9
450	9.2	6.2	4.3	14.3	11.6	9.2	14.5	13.7	12.3
500	2.1	1.4	1.0	3.4	2.7	2.1	3.6	3.3	2.9

Table 2: Same as Tab. 1 for Tevatron at $\sqrt{s} = 1.96\text{TeV}$.

For Tevatron and LHC, our approximate NNLO cross section leads to a cross section increase of 9% compared to the NLO predictions, which translates into higher exclusion limits for squark masses. Moreover, with our approximate NNLO result we have found significantly improved stability with respect to variation of the renormalization and factorization scale (keeping $\mu_r = \mu_f$). This leads to a residual theoretical uncertainty of 3% plus a (largely uncorrelated) error due to the parton luminosity depending on the particular PDF set.

As a possible extension as far as the study of QCD corrections is concerned we would like to mention bound-state effects for squark pair-production at hadron colliders, which depend on the particular color and angular momentum quantum numbers of the $\tilde{q}\tilde{q}$ -pair. This would allow the resummation of the Coulomb corrections to all orders. From similar recent work for top-quark pairs [25, 26] we would expect a shift of the total cross section by $O(1\%)$ due to these bound state corrections.

Acknowledgments

We would like to thank T. Plehn for discussions and help with the PROSPINO code [12]. The Feynman diagrams have been prepared with AXODRAW [27] and for numerical integrations the CUBA-library [28] has been used. We acknowledge support by the Helmholtz Gemeinschaft under contract VH-NG-105 and in part by the Deutsche Forschungsgemeinschaft in Sonderforschungsbereich/Transregio 9.

Appendix A: Useful formulae

For the partonic cross section one can distinguish the following subprocesses for squark pair-production according to the initial flavors and chiralities:

$$q\bar{q} \rightarrow \tilde{q}_R\tilde{\bar{q}}_R, \quad q = u, d, s, c, b, \quad (\text{A.1})$$

$$q\bar{q} \rightarrow \tilde{q}_R\tilde{\bar{q}}_L, \quad q = u, d, s, c, b, \quad (\text{A.2})$$

$$q\bar{q} \rightarrow \tilde{Q}_R\tilde{\bar{Q}}_R, \quad q, Q = u, d, s, c, b, \quad q \neq Q, \quad (\text{A.3})$$

$$q\bar{Q} \rightarrow \tilde{q}_R\tilde{\bar{Q}}_R, \quad q, Q = u, d, s, c, b, \quad q \neq Q, \quad (\text{A.4})$$

$$q\bar{Q} \rightarrow \tilde{q}_R\tilde{\bar{Q}}_L, \quad q, Q = u, d, s, c, b, \quad q \neq Q. \quad (\text{A.5})$$

The same processes are possible if one replaces the chirality index R with L and vice versa. The process (A.1) proceeds via gluon exchange in the s -channel and gluino exchange in the t -channel, the process (A.3) only via gluon exchange, and the processes (A.2), (A.4), and (A.5) only via gluino exchange. The corresponding Born cross sections are given by

$$\begin{aligned} \sigma(q\bar{q} \rightarrow \tilde{q}_R \bar{\tilde{q}}_R) = & \frac{2\pi\alpha_s^2}{27s} \left[\beta^3 + \beta \left(1 + \frac{2(m_{\tilde{g}}^2 - m_{\tilde{q}_R}^2)}{s} \right) + 2 \frac{(m_{\tilde{g}}^2 - m_{\tilde{q}_R}^2)^2 + m_{\tilde{g}}^2 s}{s^2} L_1 \right. \\ & \left. - 6\beta - 3 \left(1 + \frac{2(m_{\tilde{g}}^2 - m_{\tilde{q}_R}^2)}{s} \right) L_1 \right], \end{aligned} \quad (\text{A.6})$$

$$\sigma(q\bar{q} \rightarrow \tilde{q}_R \bar{\tilde{q}}_L) = \frac{2\pi\alpha_s^2}{9} \frac{m_{\tilde{g}}^2}{s} \frac{\sqrt{(m_{\tilde{q}_R}^2 + m_{\tilde{q}_L}^2 - s)^2 - 4m_{\tilde{q}_R}^2 m_{\tilde{q}_L}^2}}{(m_{\tilde{g}}^2 - m_{\tilde{q}_L}^2)(m_{\tilde{g}}^2 - m_{\tilde{q}_R}^2) + m_{\tilde{g}}^2 s}, \quad (\text{A.7})$$

$$\sigma(q\bar{q} \rightarrow \tilde{Q}_R \bar{\tilde{Q}}_R) = \frac{2\pi\alpha_s^2}{27s} \beta^3, \quad (\text{A.8})$$

$$\begin{aligned} \sigma(q\bar{Q} \rightarrow \tilde{q}_R \bar{\tilde{Q}}_R) = & -\frac{2\pi\alpha_s^2}{9s} \left[2 \frac{\sqrt{(m_{\tilde{q}_R}^2 + m_{\tilde{Q}_R}^2 - s)^2 - 4m_{\tilde{q}_R}^2 m_{\tilde{Q}_R}^2}}{s} \right. \\ & \left. + \left(1 + \frac{2m_{\tilde{g}}^2 - m_{\tilde{q}_R}^2 - m_{\tilde{Q}_R}^2}{s} \right) L_1 \right], \end{aligned} \quad (\text{A.9})$$

$$\sigma(q\bar{Q} \rightarrow \tilde{q}_R \bar{\tilde{Q}}_L) = \frac{2\pi\alpha_s^2}{9} \frac{m_{\tilde{g}}^2}{s} \frac{\sqrt{(m_{\tilde{q}_R}^2 + m_{\tilde{Q}_L}^2 - s)^2 - 4m_{\tilde{q}_R}^2 m_{\tilde{Q}_L}^2}}{(m_{\tilde{g}}^2 - m_{\tilde{Q}_L}^2)(m_{\tilde{g}}^2 - m_{\tilde{q}_R}^2) + m_{\tilde{g}}^2 s} \quad (\text{A.10})$$

with $m_{\tilde{q}}$, $m_{\tilde{q}_{R/L}}$, and $m_{\tilde{Q}_{R/L}}$ denoting squark masses and L_1 is defined in Eq. (7).

We have parametrized the numerical result of PROSPINO [12] for the NLO scaling functions in $f_{gg}^{(10)}$, $f_{qq}^{(10)}$, and $f_{q_i q_j}^{(10)}$ by a fit (accurate at the per mille level), where the fit function $h(\beta)$ in Eqs. (9) and (10) reads

$$\begin{aligned} h(\beta) = & \beta \left[a_1 + a_2 \beta + a_3 \beta^2 \log(8\beta^2) + a_4 \beta^3 \log(8\beta^2) \right. \\ & + a_5 \frac{1}{\sqrt{1+\eta}} \log^2(1+\eta) + a_6 \frac{1}{\sqrt{1+\eta}} \log(1+\eta) + a_7 \frac{1}{1+\eta} \log\left(\frac{1+\beta}{1-\beta}\right) \\ & + a_8 x \log^2(\eta) + a_9 x \log(\eta) + a_{10} x^2 \log^2(\eta) + a_{11} x^2 \log(\eta) \\ & + a_{12} x^3 \log^2(\eta) + a_{13} x^3 \log(\eta) + a_{14} x^4 \log^2(\eta) + a_{15} x^4 \log(\eta) \\ & \left. + a_{16} x^5 \log^2(\eta) + a_{17} x^5 \log(\eta) \right], \end{aligned} \quad (\text{A.11})$$

and x is defined as

$$x = \frac{\eta}{(1+\eta)^2}, \quad \beta = \sqrt{\frac{\eta}{1+\eta}}. \quad (\text{A.12})$$

We present the coefficients of $h(\beta)$ in Tab. 3. For our choice of squark and gluino masses, $m_{\tilde{q}} = 400\text{GeV}$ and $m_{\tilde{g}} = 500\text{GeV}$, the fit is accurate at the per mille level. However, the squark mass dependence of the coefficients a_i is weak, so that for the ratio $m_{\tilde{g}} = 1.25m_{\tilde{q}}$, the fit may even be used in the whole range $m_{\tilde{q}} = 200\text{GeV} \dots 1\text{TeV}$ with a an error of less than 1%, the maximum error being 0.7% at the lowest values of $m_{\tilde{q}}$.

a_i	$f_{gg}^{(10)}$	$f_{qq}^{(10)}$	$f_{q_i q_j}^{(10)}$
a_1	0.49100112	0.14999587	0.14422667
a_2	-1.91412644	7.76393459	1.63082127
a_3	-0.60192840	0.67354296	-0.23767546
a_4	1.55221239	-4.45797953	-0.59322814
a_5	-0.00562902	0.01846674	-0.00167924
a_6	0.05091553	-0.16690138	0.01653721
a_7	0.96279970	-4.26865285	-0.88130118
a_8	-0.32470009	0.61779585	0.07212666
a_9	-0.12126013	1.09469670	0.36722998
a_{10}	-0.50416435	0.85492550	0.03809051
a_{11}	0.70967285	-0.61743437	-0.48810751
a_{12}	3.99890940	-8.15404313	-0.02789299
a_{13}	-9.83101731	4.99311643	2.37790285
a_{14}	-16.88306230	44.33618984	-0.60307995
a_{15}	52.83111706	-26.25150811	-7.30816582
a_{16}	20.74447249	-93.67735527	1.80344717
a_{17}	-99.69494837	57.74025069	9.30489420

Table 3: Coefficients for the fit functions (9), (10) and (A.11) for $m_{\tilde{q}} = 400\text{GeV}$ and $m_{\tilde{g}} = 500\text{GeV}$.

Note that the values for the constant a_1 for quark-anti-quark scattering in Tab. 3 can also be used for other ratios of $r_q = m_{\tilde{g}}/m_{\tilde{q}}$ to very good accuracy because of the weak squark mass dependence at NLO. Since $a_1 = a_1(r_q)$, we can be extract from Tab. 3 for the value of a_1 at $r_q = 1.25$:

$$a_1(r_q) = \frac{1681}{400} \frac{r_q^2}{(1+r_q^2)^2} a_1(r_q = 1.25). \quad (\text{A.13})$$

This is due to $\lim_{\beta \rightarrow 0} h(\beta)/\beta = a_1$ and Eq. (21).

References

- [1] K. Peters, (2008), 0810.2353
- [2] D0 collaboration, V.M. Abazov et al., Phys. Lett. B660 (2008) 449, 0712.3805
- [3] CDF collaboration, T. Adams, (2008), 0808.0728
- [4] ATLAS collaboration, CERN-LHCC-1999-015, ATLAS-TDR-015 (1999), (available at <http://cdsweb.cern.ch/>)
- [5] CMS collaboration, G.L. Bayatian et al., J. Phys. G34 (2007) 995

- [6] W. Beenakker et al., Nucl. Phys. B492 (1997) 51, hep-ph/9610490
- [7] S. Moch and P. Uwer, Phys. Rev. D78 (2008) 034003, 0804.1476
- [8] S. Moch and P. Uwer, Nucl. Phys. Proc. Suppl. 183 (2008) 75, 0807.2794
- [9] E. Laenen, (2008), 0809.3158
- [10] A. Kulesza and L. Motyka, (2008), 0807.2405
- [11] M. Czakon and A. Mitov, (2008), 0811.4119
- [12] W. Beenakker, R. Höpker and M. Spira, (1996), hep-ph/9611232
- [13] H. Contopanagos, E. Laenen and G. Sterman, Nucl. Phys. B484 (1997) 303, hep-ph/9604313
- [14] S. Catani et al., Nucl. Phys. B478 (1996) 273, hep-ph/9604351
- [15] S. Moch, J.A.M. Vermaseren and A. Vogt, Nucl. Phys. B726 (2005) 317, hep-ph/0506288
- [16] W.L. van Neerven and A. Vogt, Nucl. Phys. B588 (2000) 345, hep-ph/0006154
- [17] N. Kidonakis et al., Phys. Rev. D64 (2001) 114001, hep-ph/0105041
- [18] S. Moch, J.A.M. Vermaseren and A. Vogt, Nucl. Phys. B688 (2004) 101, hep-ph/0403192
- [19] A. Vogt, S. Moch and J.A.M. Vermaseren, Nucl. Phys. B691 (2004) 129, hep-ph/0404111
- [20] J.A. Aguilar-Saavedra et al., Eur. Phys. J. C46 (2006) 43, hep-ph/0511344
- [21] W. Beenakker et al., Nucl. Phys. B515 (1998) 3, hep-ph/9710451
- [22] D0 collaboration, V.M. Abazov et al., (2008), 0811.0459
- [23] P.M. Nadolsky et al., Phys. Rev. D78 (2008) 013004, 0802.0007
- [24] A.D. Martin et al., Phys. Lett. B652 (2007) 292, 0706.0459
- [25] K. Hagiwara, Y. Sumino and H. Yokoya, Phys. Lett. B666 (2008) 71, 0804.1014
- [26] Y. Kiyo et al., (2008), 0812.0919
- [27] J.A.M. Vermaseren, Comput. Phys. Commun. 83 (1994) 45
- [28] T. Hahn, Comput. Phys. Commun. 168 (2005) 78, hep-ph/0404043